Computational and Structural Biotechnology Journal 21 (2023) 3522–3531

Contents lists available at ScienceDirect

Computational and Structural Biotechnology Journal

journal homepage: www.elsevier.com/locate/csbj

Research Article

A small non-interface surface epitope in human IL18 mediates the dynamics and self-assembly of IL18-IL18BP heterodimers

Yılmaz Yücehan Yazıcı [a], Serkan Belkaya [a,1], Emel Timucin [b,*,1]

[a] İhsan Doğramacı Bilkent University, Department of Molecular Biology and Genetics, Ankara 06800, Turkey
[b] Acibadem University, School of Medicine, Department of Biostatistics and Medical Informatics, Istanbul 34752, Turkey

ARTICLE INFO

Article history:
Received 26 March 2023
Received in revised form 16 June 2023
Accepted 29 June 2023
Available online 1 July 2023

Keywords:
Interleukin-18
Interleukin-18 binding protein
Protein-protein interactions
Self-assembly
Molecular dynamics simulations

ABSTRACT

Interleukin 18 (IL18) is a pro-inflammatory cytokine that modulates innate and adaptive immune responses. IL18 activity is tightly controlled by the constitutively secreted IL18 binding protein (IL18BP). PDB structures of human IL18 showed that a short stretch of amino acids between 68 and 81 adopted a disordered conformation in all IL18-IL18BP complexes while adopting a 3_{10} helical structure in other IL18 structures, including the receptor complexes. The C74 of human IL18, which was reported to form a novel intermolecular disulfide bond in the human tetrameric assembly, is also located in this short epitope. These observations reflected the importance of this short surface epitope for the structure and dynamics of the IL18-IL18BP heterodimers. We have analyzed all known IL18-IL18BP complexes in the PDB by all-atom MD simulations. The analysis also included two computed complex models adopting a helical structure for the surface epitope. Heterodimer simulations showed a stabilizing impact of the small surface region at the helical form by reducing flexibility of the complex backbone. Analysis of the symmetry-related human IL18-IL18BP tetramer showed that the unfolding of this small surface region also contributed to the IL18-IL18BP stability through a completely exposed C74 sidechain to form an intermolecular disulfide bond in the self-assembled human IL18-IL18BP dimer. Our findings showed how the conformation of the short IL18 epitope between amino acids 68 and 81 would affect IL18 activity by mediating the intermolecular interactions of IL18.

© 2023 The Authors. Published by Elsevier B.V. on behalf of Research Network of Computational and Structural Biotechnology. This is an open access article under the CC BY-NC-ND license (http://creativecommons.org/licenses/by-nc-nd/4.0/).

1. Introduction

IL18, a proinflammatory cytokine belonging to the IL-1 superfamily, protects its host against infections and regulates innate and adaptive immune responses [2]. Dysregulation of its activity has been implicated in many immune-related diseases in humans [22,25,60]. IL18 signaling is tightly regulated through different mechanisms [35,61], one of which involves regulation of the availability of IL18 through a constitutively secreted decoy protein termed as IL18 binding protein (IL18BP) [3,25,45]. Inherited human IL18BP deficiency was reported to predispose to fulminant viral hepatitis due to uncontrolled immunopathological activity of IL-18 in the liver [7]. IL18BP is not only conserved across the animal kingdom, but its orthologs have also been found in poxviruses such as Molluscum contagiosum, variola, vaccinia, and Yaba-like disease viruses (YLDV) [8,43,50,59].

The structure of IL18BPs has been extensively studied [57]. A recent crystallization study that captured the human IL18-IL18BP complex [12] reported that human IL18BP adopted the same immunoglobulin-like β-sandwich fold of viral IL18BPs [45]. The binding interface of the human IL18-IL18BP heterodimer has overlapped with those formed with viral IL18BPs [12,29], confirming the inhibition mechanism of host and viral IL18BPs. Host and viral IL18BPs compete with the IL18 receptor α (IL18Rα) over a hydrophobic surface of approximately 2 nm^3 [30], leading to the sequestration of human IL18 (hIL18).

Despite the common inhibition mechanism, the IL18-IL18BP heterodimers can form distinct tetrameric assemblies by disulfide contacts. For instance, the heterodimers formed by the decoy (IL18BP) of the Yaba-like disease virus (YLDV) can self-assemble into a tetrameric state through an intermolecular sulfide contact

* Corresponding author.
E-mail address: emel.timucin@acibadem.edu.tr (E. Timucin).
[1] These authors contributed equally.

https://doi.org/10.1016/j.csbj.2023.06.021
2001-0370/© 2023 The Authors. Published by Elsevier B.V. on behalf of Research Network of Computational and Structural Biotechnology. This is an open access article under the CC BY-NC-ND license (http://creativecommons.org/licenses/by-nc-nd/4.0/).

between the C132s of the YLDV decoys (PDB ID: 4eee) [29]. The recent human complex (PDB ID: 7al7) has also been shown to form a symmetry-related tetrameric assembly through an intermolecular disulfide contact between the C74 of IL18 and C131 of IL18BP [12]. Inspection of hIL18 structures in PDB showed a rigid binding interface of IL18 that did not change its conformation upon binding to the protein partners such as IL18Rα/β, anti-IL18, and IL18BP [55,57]. However, a short stretch of amino acids between 68 and 81 that is orthogonal to the IL18BP binding site adopted different folds depending on the quaternary structure of IL18. This region is either completely missing or highly flexible in all IL18-IL18BP complexes. At the same time, it was folded into a compact 3_{10} helical form in the free and other complex forms of hIL18. This region also holds the cysteine residue at the 74*th* location involved in a novel intermolecular disulfide contact in the human tetrameric complex, reflecting this short epitope's importance for the self-assembly of the heterodimers. Altogether, PDB structures of hIL18 structures underscore the importance of the short surface epitope of IL18 between 68 and 81 for controlling its activity by affecting the heterodimer conformation/stability and self-assembly.

Undeniably, these structural findings on the IL18-IL18BP complexes, either of host or viral origin, provide valuable insights into the mechanism of inhibition of IL18 by IL18BPs. However, they can only vaguely describe the conformational dynamics of the complexes, representing a single snapshot of a plethora of possible conformations. Thus, these data solely relying on the static models fail to address whether and how the short surface epitope can affect heterodimer stability and self-assembly. Molecular dynamics (MD) simulations, a widely used computational methodology to sample the conformational space of biomolecules [19], could be of use in analyzing the dynamics of IL18-IL18BP complexes, focusing on the impact of the conformation of the IL18 epitope between residues 68–81.

In this study, we analyzed all PDB complexes of IL18-IL18BP and two computed models that adopted distinct conformations for the surface region by all-atom MD simulations. Dimer simulations showed a stabilizing impact of the small surface region at the helical form by reducing flexibility. Analysis of the human IL18-IL18BP dimer showed that the unfolding of this small surface region could also contribute to the complex stability by promoting tetramer formation. These findings altogether reflect the importance of the conformation of the short IL18 epitope between 68 and 81 for IL18–IL18BP heterodimer stability and self-assembly.

2. Methods

2.1. Homology modeling of the core region of human IL18BP

The core region of the human IL18BP (UniProt ID: O95998) encompassing the residues from 20 to 170 was predicted by MODELLER v9.25 [14] using the YLDV IL18BP structure (PDB ID: 4EKX) as the template. The best structure was selected based on the discrete optimized protein energy score [34]. The final model was confirmed to be free of Ramachandran outliers.

2.2. Docking-based prediction of the human IL18-IL18BP complex

Docking runs were performed using the PDB structures of IL18 (PDB IDs: 3wo2, 3wo3, 3wo4, and 4r6u) [55,57] as receptor and the homology model of IL18BP as ligand. Before docking, missing regions in the PDB structures were predicted by MODELLER [14]. First, a rigid docking algorithm named ClusPro [27] was used to predict the complex. Top-scoring ClusPro predictions were superimposed to identify the predominant binding interface and the amino acids that lined this interface. Next, we used this information in the HADDOCK calculations that were performed by keeping the interface loops flexible [62]. The representative structure of the top HADDOCK cluster of each run, which was performed for four different IL18 structures, was inspected, and the final model was selected based on docking scores.

2.3. AlphaFold2 prediction of human IL18-IL18BP complex

Human IL18BP was predicted in its free form and also in the IL18 complex form by AlphaFold2 [4,15,24,39]. MSAs were generated by MMseq2 [40,52] using the databases of UniRef100 [53] and PDB70 05Sep15 which is a clustered version of PDB [51]. The final model was relaxed by the AMBER force field [13]. The top-ranked structure was selected based on residue confidence scores (pIDDT) and error plots (PAE).

2.4. Molecular dynamics simulations

A total of five heterodimers, three from PDB (PDB IDs: 7al7, 3f62, and 4ekx) and two from computational predictions were included in this study. The viral tetramer from YLDV (4eee) and the symmetry-related human tetramer were also modeled in the presence (S-S) and absence of (-SH) the intermolecular disulfide bonds. Missing non-terminal regions were modeled by MODELLER [14], and nonstandard residues were removed from the structures. Overall, nine different IL18-IL18BP complexes were generated and placed in the center of a cubic water box with a padding distance of 10 Å. Solvated systems were neutralized to a final concentration of 0.15 M, using Na^+ and Cl^- counter ions.

The resulting systems were simulated by the GROMACS algorithm [1,6,32,56] with the CHARMM36 force field including the correction map [20] Water molecules were treated explicitly by the TIP3P model [23]. Periodic boundary conditions and a time-step of 2 fs were applied for all simulations. Particle-mesh Ewald summation method was used to compute the long-range electrostatic interactions with a grid spacing of 1.2 Å and a cut-off of 12 Å for short-range interactions [11]. All systems were energy-minimized in 40,000 steps by the steepest descent method and equilibrated by an NVT ensemble with a Berendsen thermostat at 310 K. After equilibration, production runs were carried out using an NPT ensemble with a Parrinello-Rahman pressure coupling at 1 atm and 310 K. System details are given in Table S1.

2.5. Data analysis

MD trajectories were analyzed by root mean square displacement (RMSD) and fluctuation (RMSF) of Cα atoms, the radius of gyration (R_G), solvent accessible surface area (SASA) of the complex and its subunits. Visual Molecular Dynamics (VMD) was used to visualize the trajectories and structures [21]. MDAnalysis was used to plot all-to-all RMSD heatmaps [16,37]. Essential dynamics of the systems were extracted by principal component analysis (PCA) using Bio3D [17]. The method uses the mass-weighted Cartesian coordinates of the Cα atoms, which can be converted into a covariance matrix of C_{ij} as follows:

$$C_{ij} = \langle (q_i - \langle q_i \rangle)(q_j - \langle q_j \rangle) \rangle \quad (1)$$

wherein q_i and q_j represent the internal coordinates of atoms i and j, $\langle \ldots \rangle$ describes the ensemble average. Later, principal components are calculated by eigendecomposition on the C_{ij}. A two-dimensional free-energy landscape (FEL) was also constructed using the first two principal components as follows:

$$\Delta G(x) = -k_B T ln \frac{P(V_x)}{P_{max}(V)} \quad (2)$$

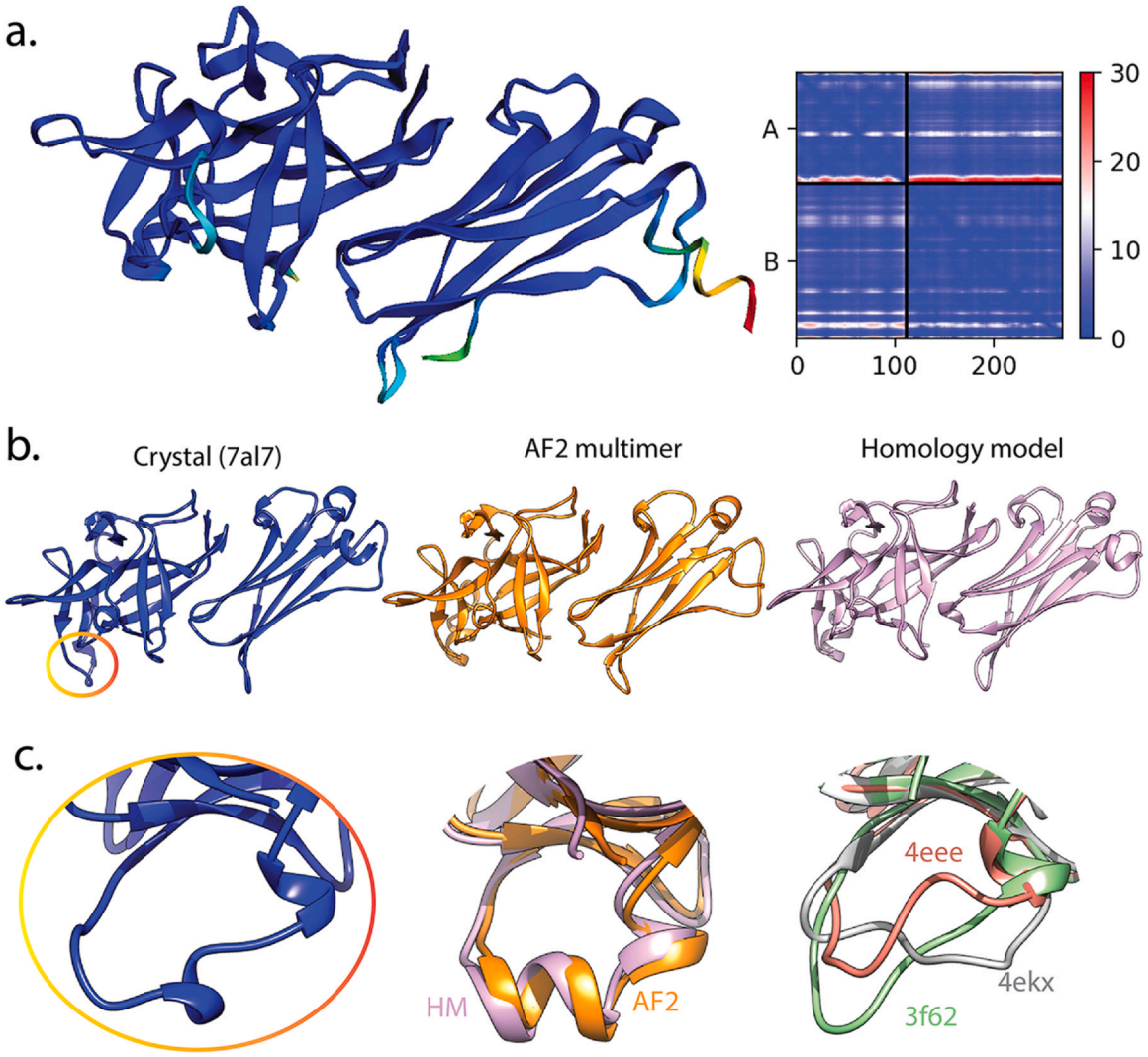

Fig. 1. (a) Panel shows the computed complex structure of human IL18-IL18BP by AF2 that was colored according to residue confidence score (red: pIDDT < 50, yellow: pIDDT < 60, green: pIDDT < 70, cyan: pIDDT < 80, blue: pIDDT < 90). A predicted aligned error (PAE) plot is also given. Chain A shows IL18BP, and B shows IL18. (b) Panel shows the superimposed structures of human crystal complex, AF2 multimer, and docking-based predictions. RMSD values for this comparison are given in Table 1. (c) Panel shows the small region with different conformations in the complexes analyzed in this study.

wherein k_B is the Boltzmann constant, and T is the absolute temperature. $P(V_x)$ and $P_{max}(V)$ are probabilities from the MD data, with $P_{max}(V)$, representing the most probable state.

3. Results

3.1. Computational predictions capture the experimental structure of human IL18-IL18BP complex

We have modeled the human IL18-IL18BP complex structure from scratch by AlphaFold2 and molecular modeling methods. The AF2 predicted structure showed high confidence scores for almost every amino acid and low positional error, particularly for the dimer interface (Fig. 1a). RMSD of Cα- and all-atoms of the AF2 computed structure were below 2 Å for both subunits (Fig. 1b and Table 1). Considering that the AF2 prediction was made without any template (no-template mode) and prior to April 2022, when the human crystal complex was released in PDB [12], the accuracy of the predicted structure is noteworthy.

The second model that was obtained by docking the hIL18 structure from PDB to the homology model of human IL18BP was also an accurate model (Fig. 1b and Table 1). Comparison of two PDB structures of human IL18, the one (PDB ID: 3wo2) [55], which was recruited to docking and the reference structure (PDB ID: 7al7), showed some variations as well. The Cα and all-atom RMSD values for this comparison ranged between 1.8 and 2.7 Å, respectively (Table 1). Comparison of the homology model of human IL18BP with the experimental structure (7al7) showed comparable RMSD values (Table 1), suggesting a close error margin of the homology modeling to experimental predictions. Overall, comparing the computed models with the experimental reference structure (PDB ID: 7al7) confirmed the capacity of both AF2 and comparative modeling/docking-based predictions for capturing the human IL18-IL18BP complex. We also compared the AF2 and homology model predicted complexes. A comparison of the predicted IL18 backbones showed a

Table 1
Comparison of the computed models against the experimental structure.

	IL18		IL18BP	
	Cα	All atom	Cα	All atom
AF2	1.184	2.017	1.482	1.935
HM-Dock	1.815**	2.708**	1.078	1.799

Reference structure: 7al7.
**IL18 was obtained from 3wo2 for the docking study.

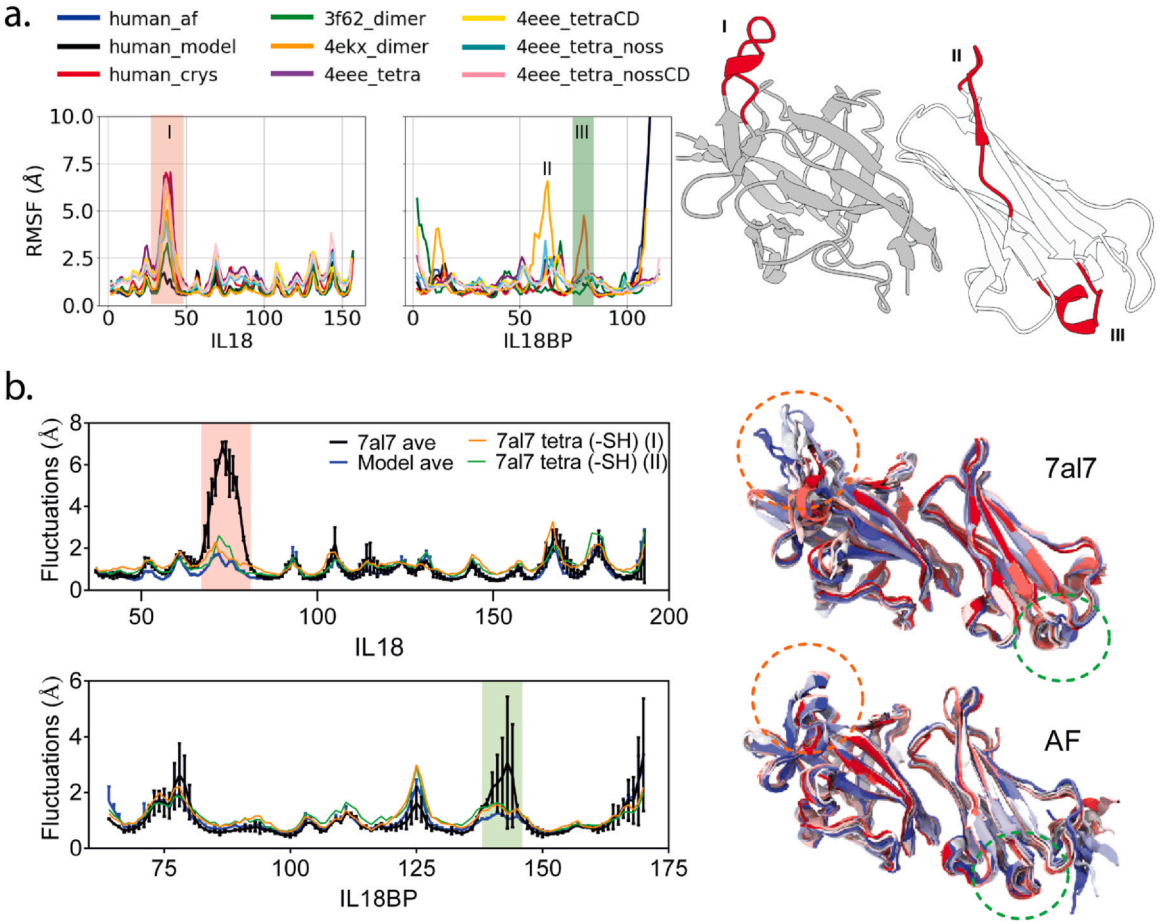

Fig. 2. (a) Cα fluctuations calculated for the last 200 ns. Human AF: blue, human model: black, human crystal: red, 3f62: green, 4ekx: orange, 4eee-SS AB chains: purple, 4eee-SS CD chains: yellow, 4eee-SH AB chains: teal, 4eee-SH CD chains: pink. The complex structure illustrates the mobile regions colored red. (b) Average fluctuations of the human complexes for the last 200 ns, crystal structure (black), and computed models (blue). Two replicate simulations were used for both structures, with error bars representing standard deviation. Fluctuations of the human tetramer were shown in orange and green lines representing each subunit in the 2:2 complex. The residue index was set according to the 7al7 structure. Shaded areas mark highly mobile regions in the reduced trajectory of the dimer structures of crystal complex (7al7) and the AF2 computed model.

Cα-RMSD of 1.1 Å, whereas comparison of the IL18BP backbones showed a RMSD value of 1.0 Å.

As intended, the surface region of hIL18 corresponding to a short stretch of amino acids between 68 and 81 was the most structurally divergent region in the computational models (Fig. 1c). Computational models adopted a compact 3_{10} helix (Fig. 1c), which is the dominant conformation of hIL18 in the PDB ensemble. In contrast, the IL18 in the recently resolved human complex (7al7) was disordered (Fig. 1c). The C74, which is one of the cysteines reported to form a novel intermolecular disulfide bridge in the human complex, is also located in this helix [12]. To test the contribution of the conformation of this surface region holding the C74, we have included the computed models of human IL18-IL18BP complexes by AF2 and docking models that have the compact helical fold for the surface region in our study (Fig. 1c).

To analyze the contribution of different oligomeric states, we have directly recruited the tetra-partite assembly of the hIL18 and IL18BP from YLDV (PDB ID: 4eee) (Fig. S1b). Because the human tetramer did not have any experimental coordinates, we used an initial MD simulation to relax the constructed human tetramer, which was generated after a symmetry operation of the crystal heterodimer (7al7) and by forming two symmetric disulfide bonds between C74 of hIL18 and C131 of hIL18BP (Fig. S1c). To scrutinize the contribution of the intermolecular disulfide bonds in the tetra-partite assemblies, we have generated the tetramers with and without the intermolecular bond(s). Overall, nine MD systems representing all known variants of IL18-IL18BP complexes were analyzed to address how the complex dynamics are affected by (i) different decoys, (ii) different hIL18 surface structures of the region between 68 and 81, and (iii) different oligomeric states.

3.2. Origins of the IL18 and IL18BP affect the backbone mobility and shape of the complexes

All-to-all RMSD plots showed that the human IL18-IL18BP complex from the crystallization study [12] showed the highest backbone mobility in the repeated runs (Fig. S1a). This change approximately corresponded to a Cα-RMSD of 8 Å. The viral decoy from ectromelia virus (3f62) also showed high mobility (Fig. S1a). Contrary to these two complexes, the heterodimers showed almost rigid backbones.

Shape analysis was conducted by monitoring the R_G and SASA of the dimeric and monomeric forms of the complexes (Fig. S2). Both the R_G and SASA measurements of hIL18 were more uniform than those of the decoys (Fig. S2), which is a reasonable outcome given the difference in the origins of the decoy structures. Explicitly, the R_G and SASA values of the hIL18 ranged between 15 and 16 Å and 80–90 nm^2, respectively, whereas slightly wider ranges of 14–16 Å and 60–80 nm^2 were sampled for the decoy structures. Overall, the shape analysis monitored by both SASA and R_G reflected a variation

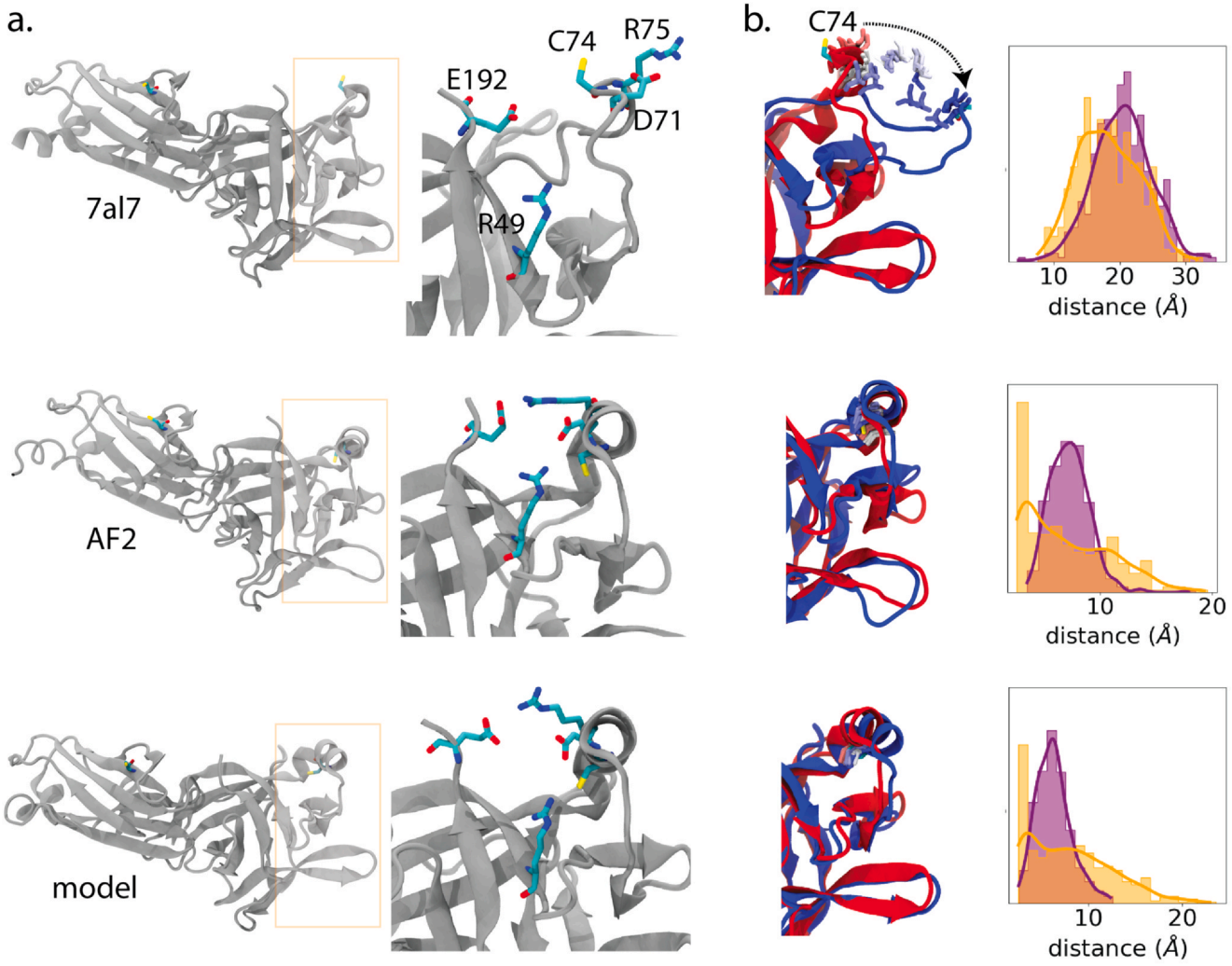

Fig. 3. Dynamics of the small surface helix in the human complexes. First row in both (a) and (b) illustrates the crystal complex, and the second and third rows show the computational models. The movement of the helix/loop is shown in the second column. The red color indicates the starting conformation and the blue shows the conformation after 300 ns. Two salt bridge contacts were shown for the starting structure alongside the C74. Distance distributions of the salt bridges were shown (orange: E192-R75, purple: D71-R49). Residue numbering follows the 7al7 structure.

in the structure of the complex and its subunits depending on the origin of the decoy and hIL18.

The complex formed with the ectromelia decoy was slightly more compact than the rest, displaying an average radius of 20.5 Å (Fig. S2a, green line). Despite this small but notable difference in the R_G measurements, SASA of the same complex was measured to be around 150 nm^2, which was comparable to other complexes (Fig. S2b). The inconsistency between R_G and SASA is likely to be resulted from the fact that the shape of the heterodimers and possibly the monomers are not ideally globular (Fig. 1), rendering R_G measurements less informative about the shape than SASA measurements [49]. Notably, the hIL18 in the human complex showed parallel changes in the R_G and SASA measurements (Fig. S2). Taken together with the change in the all-to-all RMSD plot of this complex (Fig. 1), the upward movements of both R_G and SASA of the hIL18 implied a loosened IL18 in the human heterodimer (Fig. S2). On the other hand, the same complex from the computed models did not show any R_G or SASA changes, implying a link between the backbone dynamics of the human heterodimer and conformation of the surface epitope encompassing the residues 68–81.

3.3. Mobility of IL18 is dependent on the conformation of the small surface epitope

Cα fluctuations were computed for the last 200 ns of the simulations (Fig. 2a). Three interior regions, one from the IL18 (Fig. 2a, I) and two from the decoy structures (Fig. 2a, II–III), showed high fluctuations. These regions corresponded to the short surface epitope (region I) in IL18 that adopted different conformations in the PDB structures (Fig. 1c) and two surface loops in the decoy structures, termed the DE and EF loops, respectively [12].

Region I showed high fluctuations for all IL18 structures except the computed models (Fig. 2a). This mobile region corresponding to the small surface helix almost froze in the computational models, fluctuating less than 2 Å. The computed models did not show any increased fluctuations almost for the entire complex except the C-termini of their decoys (Fig. 2a). Viral decoys also showed high fluctuations for region II and the human decoy for region III (Figs. 2a and S4).

We also conducted essential dynamics and free energy landscape analyses to extract essential dynamics and dominant conformations of the systems, respectively (Fig. S3). In line with the fluctuation analysis (Fig. 2), essential dynamics based on the first two principal

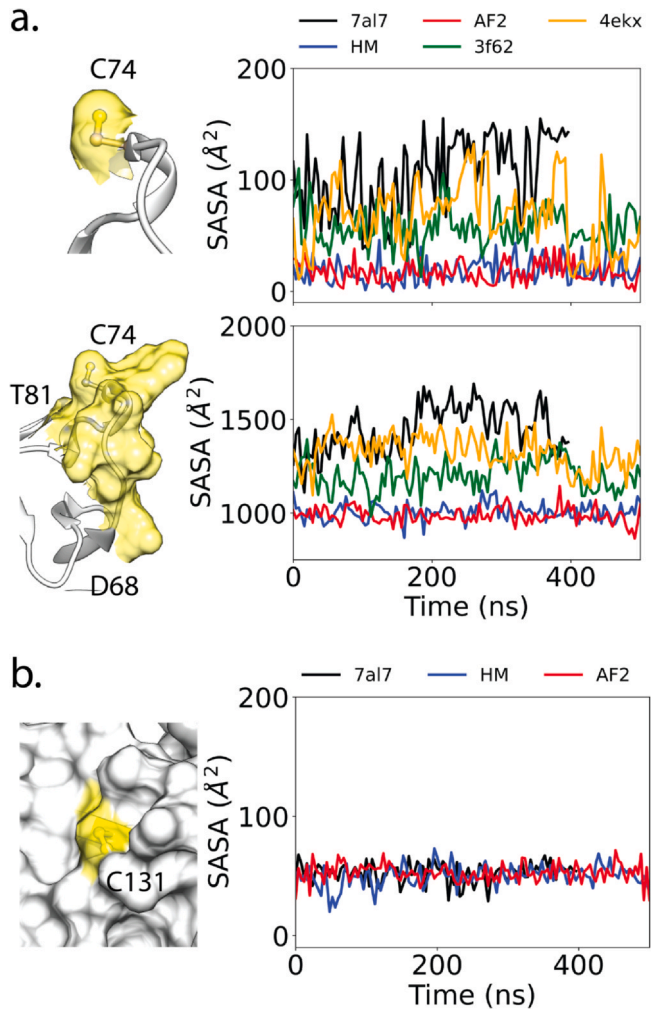

Fig. 4. (a) Panel shows SASA changes over time for the 74*th* position and the entire epitope holding this position of hIL18. (b) Panel shows the SASA changes over time for the C131 of hIL18BP, which was proposed to participate in a novel intermolecular disulfide contact with the C74 of hIL18.

components (pcs) suggested that the IL18 structures in the computational models sampled a limited conformational space (Fig. S1). The wide pc1–pc2 planes of the host decoy from the computed models were likely to be due to the mobility of their C-termini because the rest of the complex did not fluctuate more than 3 Å in the computed models (Figs. 2 and S1). The IL18 in the human crystal complex showed the widest pc1–pc2 plane suggesting a larger conformational space sampled by the crystal complex of the human heterodimer compared to other heterodimers. RMSF and essential dynamics analyses also showed that the tetrameric structures were not destabilized by removal of the intermolecular disulfide contacts. Instead, they showed highly rigid backbones that were comparable to those in the presence of intermolecular disulfide contacts (Figs. 2, S3, and S4).

We computed average fluctuations of the human complex using two replicates of the human crystal complex (7al7) and of two computed models (Fig. 2b). Mean fluctuations were generally higher in the crystal complex than the computed models, particularly for the short surface epitope (Fig. 1c). We also observed high mobility of region III in the decoy structure of the crystal human complex. The human tetramer, which was constructed using the 7al7 heterodimer, showed particularly low mobility compared to the heterodimer form (Fig. 2b). Although both heterodimer and tetrameric forms of human complexes shared the same conformation for the short surface epitope encompassing residues from 68 to 81, reduced flexibility of the tetramer is likely to result from the steric effect of tetramerization. Overall, these analyses suggested that the initial conformation of the surface epitope affects the flexibility of region I of IL18 and region III of IL18BP (Fig. 2).

3.4. Conformation of the small surface helix mediates stability and self-assembly of heterodimers

We investigated the local structure of the short surface epitope in the human complexes (Fig. 3). Comparison of the static structures unraveled different initial conformations of two amino acids, one acidic (E192) and one basic amino acid (R75) in this region. As this region is folded into a compact helical form, these charged amino acids come in close contact with two core amino acids that are also charged (Fig. 3a). Explicitly, the guanidinium group of R75 protrudes toward the carboxylic acid group of E192. Similarly, the sidechain of D71 attracts that of R49, resulting in two salt-bridge interactions in the hIL18 structures that maintain a helical fold for the surface region (Fig. 3). These intramolecular interactions linking the short helix to the IL18 core tend to be at play when this epitope (region I) adopts the helical fold as in the computed models, however; they would be disrupted when it is disordered (Figs. 3a and S4). Two salt bridge interactions spotted in the static models were preserved in the computed models but not in the crystal structure (7al7). Distance distributions of these bonds reflected that the computed models showed an almost identical bonding pattern such that the interaction between E192 and R75 was more persistent than the one between R49 and D71 in both computed models (Fig. 3b). Altogether, these findings suggested that the initial conformation of the surface region between 68 and 81 that affects the dynamics of the IL18-IL18BP complex through stabilization of the IL18 structure by two salt bridge interactions.

The C74 that was observed to form an intermolecular disulfide bond with the human IL18-IL18BP complex [12] is found in the region I (Fig. 3a). The computed structures with a compact helical conformation for the region I have their C74 almost completely buried as such the relative accessible surface area (rASA) values were calculated 0.007 and 0.015 for the AF2 and docking models, respectively. On the other hand, the C74's sidechain is highly exposed in the crystal complex (7al7) (rASA = 0.748). Fig. 3b shows how the structure of this region in the human complexes evolved over 500 ns. The helix structure in the computed models did not move at all, maintaining their initial conformation, in which C74 is completely buried. However, the same region, which was already unfolded, moved further away from the IL18 core in the human crystal complex, completely losing two salt bridge contacts (Fig. 3b).

Fig. 4a shows the SASA of the amino acids at the 74*th* positions and the small surface region, wherein C74 is located, for five of the complexes. The cysteines at the 74*th* positions of the viral complexes (3f62 and 4ekx) were mutated to serines [28,30]. According to maximum ASA (maxASA) values of amino acids [38,47,54], a cysteine can reach an average of maxASA of 150 $Å^2$ and a serine could reach an average of 137 $Å^2$. Given these maxASA values for cysteine and serine amino acids, the 74*th* positions became completely accessible in all simulations except those of the computed models (Fig. 4a). The C74s in the computed models stayed buried throughout the simulations, implying that they were not available for any intermolecular contacts (Fig. 4a). We also tracked down the SASA of the entire region I (Fig. 4a-bottom). Taken together with the reduced trajectory of region I in the human complex (Fig. 3a), the SASA measurements of the short surface epitope confirmed a compact structure for the computed models and highly exposed conformations for the other complexes (Fig. 4a-bottom panel). We lastly measured the SASA of the other cysteine (C131) (Fig. 4b) that was reported to bind to the C74 [12]. All human decoys showed that this cysteine was partially

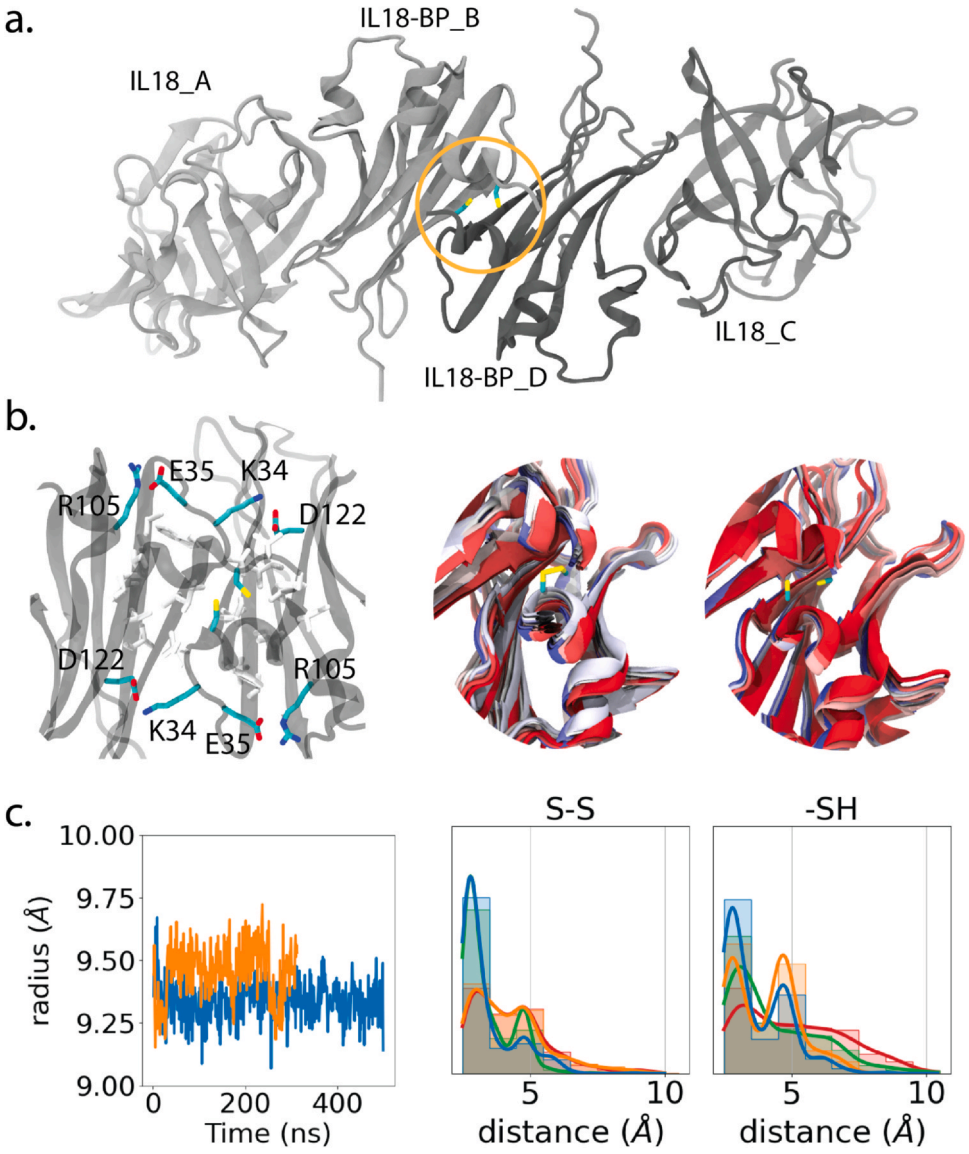

Fig. 5. (a) Panel shows the tetrameric 2:2 complex (4eee), marking the intermolecular disulfide bridge between the IL18BP chains. (b) Panel shows the interface between IL18BP chains. Two disulfide bridges (E35-R105, K34-D122) were spotted for both chains. Surrounding hydrophobic amino acids were shown by white stick models. The reduced trajectory was shown for the IL18BP symmetric interface in the presence (S-S) and absence (-SH) of the intermolecular disulfide bridge (C132-C132). (c) Analysis of the radii of the hydrophobic residues at the interface is shown in (b), and distance distributions of the salt bridges (E35-R105: orange, red; K34-D122: green, blue).

accessible, and its accessibility was not affected by a change in the complex conformation, particularly in the short IL18 epitope.

3.5. Human tetramer stability is dependent on intermolecular disulfide bonds and other interactions

In order to assess the contribution of the disulfide contacts to the dynamics of the tetramers, we modeled the tetramers in the absence and presence of intermolecular disulfide bond(s) (Fig. S1b–c). Inspection of the interface, which is contoured by symmetrical surfaces of YLDV decoys, showed that the tetrameric assembly could be stabilized not only by the disulfide bond but also by hydrophobic and ionic interactions (Fig. 5b). We analyzed the R_G of the hydrophobic cluster including I29, V31, V124, and I129, and the distance between charged amino acids, K34-D122 and E35-R105 (Fig. 5c). Results showed that the hydrophobic cluster and the distance between charged amino acids were conserved throughout the simulation in the tetramer even in the absence of the intermolecular disulfide attachment. This observation implied a less pronounced impact of the disulfide bond on the stability of the YLDV tetramer, underscoring the contribution of secondary interactions that are mediated by hydrophobic and charged amino acids.

Because the coordinates of the human tetramer were not available, we carefully constructed this tetramer from two 7al7 heterodimers and equilibrated the constructed tetramer in the presence of two disulfide bonds between C74 of hIL18 and C131 of hIL18BP. The *in-silico* constructed tetramer underwent an immediate change and then showed a stable backbone throughout the rest of the simulation (Fig. S1c). We obtained a single snapshot from the stabilized trajectory as the initial structure of the second simulation, which was carried out by removing the disulfide contacts (Fig. S1c). We inspected the symmetric tetramer interfaces focusing on the separation between the cysteines responsible for intermolecular disulfide contacts (Fig. 6). Although the cysteines were modeled in their reduced state (-SH), we observed that the human tetramer stayed intact without any drastic displacement of the subunits (Fig. S1c). Close inspection of the interface without disulfide bonds showed that only one of the cysteine pairs stayed in close proximity,

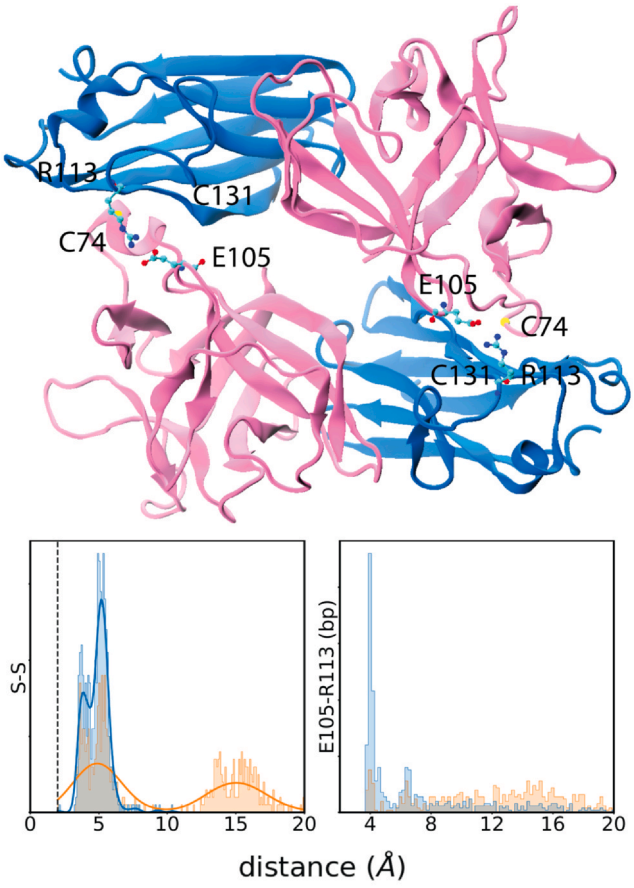

Fig. 6. Tetramer structure of hIL18 (pink) and IL18BP (blue) complex is shown, highlighting two symmetric ionic interactions between E103 and R113. Distance distributions of two cysteines and these ionic interactions were plotted for the entire trajectory. Orange and blue colors mark the left and right interfaces, respectively.

preserving one of the interfaces of the symmetry-related tetramer (Fig. 6, blue). However, the other pair became separated, resulting in disruption of the other interface (Fig. 6, orange). Akin to the YLDV tetramer, the interfaces in the human tetramer were stabilized by other contacts than disulfide bonds. In particular, E105 of hIL18 and R113 of IL18BP attracted one another, forming close interactions that showed similar distance distributions to those of the cysteine-pairs (Fig. 6).

4. Discussion

PDB structures of IL18-IL18BP complexes underlined a conformational pattern in an IL18 surface epitope depending on the quaternary structures of hIL18. This region encompasses the residues between 68 and 81 that are either unfolded or completely missing in all known IL18-IL18BP complexes [12,29,30]. In contrast, it is tightly folded into a 3_{10} helical conformation in other IL18 structures, free or complex forms (Fig. 1) [55]. This surface region was not located at the binding interface of the IL18-IL18BP heterodimers but at that of the receptor-α complex [55], rendering its conformation particularly critical for the signaling event. Furthermore, this epitope holds the C74 involved in the novel intermolecular disulfide bond in the recently described human tetramer [12]. Although these PDB structures already reflect the significance of the structure of this surface epitope for IL18-IL18BP complexes, they fail to grasp essential movements or interactions of the complexes to address the conformational changes led by the short surface epitope [5]. From this perspective, this work analyzing the IL18-IL18BP complexes by all-atom MD simulations provides a comprehensive view of whether and how the secondary structure of a hIL18 surface region affects heterodimer dynamics.

All hIL18 structures except those in the computed models showed high flexibility for this short epitope between 68 and 81, implying an association of the initial structure of this surface region with the IL18-IL18BP dynamics (Supplementary movie). The compact 3_{10} helical conformation of this short epitope stabilized the complex through two intramolecular salt-bridge interactions (Fig. 3). The computed models showed extremely low mobility for all regions except the C-termini of their decoys (Fig. 2). The C-terminus of the computational models was predicted to be slightly longer ($\sim$5 aas) than that of the decoy in the crystal structure [12]. This prediction was noted to be poor based on the confidence scores (Fig. 1a). Given the established strong correlation between the AF2 confidence scores and structural disorder [44,48], high mobility of the C-termini of the computational models would be understandable.

Nine out of fourteen hIL18 structures in PDB have adopted a compact 3_{10} helical conformation for the surface epitope encompassing residues 68–81 (PDB IDs: 3wo2, 3wo3, 3wo4, 2vxt, 4hjj, 4r6u, 4xfs, and 4xft), while it is either missing (7al7, 3f62, 4eee, 4ekx) or highly flexible (1j0s) in some structures [26]. The binary and ternary signaling complexes of IL18 also adopted the dominant helical fold for this epitope, and this helix was found at the dimer interface of the binary complex [55]. Highlighting that IL18-IL18BP complexes in PDB consistently showed a disordered structure for this epitope, which is an orthosteric site for the receptor-α [55], we surmise that the surface epitope might be unfolded due to an allosteric effect elicited upon IL18BP binding. Such allosteric changes are among the prevalent regulators of protein-protein interactions [31,33]. Further, given that this epitope holds the C74, we note that the proposed disulfide contact in the human tetramer [12] might be an allosteric disulfide bond [41]. However, these inferences were not supported by our simulations. Instead, repeated simulations of the human heterodimers showed a highly stable helical fold (Fig. 2b). Nevertheless, we note that conventional MD simulations might be limited in effectively sampling such an allosteric change [18]. To this end, enhanced sampling methods may provide further insights into whether and how IL18BP binding induces a conformational change in the surface epitope of hIL18, accessing the rarely populated conformations of the heterodimers [18,36].

Self-assembly of IL18-IL18BP heterodimers could be an important strategy to tightly regulate the activity of IL18 by host and viral decoys [29]. Hitherto, two self-assembled IL18-IL18BP heterodimers of YLDV and human decoys have been identified. Both assemblies were demonstrated to be cross-linked by intermolecular disulfide bonds, which are also among the well-known evolutionary mechanisms used for structural stabilization and functional control [58]. Only the structure of the YLDV tetramer was resolved by crystallization. In contrast, the human tetramer was not captured at the atomistic resolution but construed to form a symmetry-related assembly based on non-reducing SDS-PAGE analysis [12]. Some disulfide bonds are formed and maintained throughout proteins' life, whereas others show dynamic behavior given the reversibility of dithiol to disulfide [9,41]. The disulfide contact between C74 of IL18 and the C131 of the host IL18BP is likely to be the latter, more dynamic type. Our simulations showed a transformation of the IL18 structure in the crystal complex (7al7) to a fully accessible state of C74 (Fig. S4). Thus, the set of conformations of the human complex accessed by our MD simulations, wherein the surface epitope between 68 and 81 is fully and more exposed than the crystal conformation [12], provides novel and realistic conformations of the human heterodimer, underscoring the significance of this surface region for the self-assembly of heterodimers.

Multivalent binding, a long-known strategy for affinity enhancement, is widely encountered in protein-protein complexes

functioning in the immune system [10,42,46]. Human and YLDV decoys recruit this strategy to potentiate IL18 sequestration and tightly regulate IL18 activity through surface cysteines. A low-to-moderate sequence identity in the viral and host decoys, leading to cysteines at variable positions may account for the variability in the tetrameric assemblies of the IL18-IL18BP dimers. Human tetramer has intermolecular disulfide contacts that are formed between IL18 and IL18BP, resulting in a grid-like organization of dimers (Fig. 5) [12]; unlike the YLDV tetramer, which is formed by a disulfide attachment between C132s of the YLDV decoys leading to a side-by-side spatial arrangement of the dimers [29]. Intermolecular contacts other than disulfide bonds were found at the interface of the YLDV tetramer. A cluster of hydrophobic amino acids has contributed to YLDV tetramer stability along with four symmetric salt bridges because removing the disulfide bond did not affect the interface (Fig. 5b–c). While the hydrophobic cluster has been previously characterized by extensive mutagenesis analysis [29], persistent salt bridge interactions and their contribution to tetramer stability have been revealed by this study.

The human tetramer also showed additional contacts at the interface, such as the salt bridge interaction between the E105 of hIL18 and the R113 of lL18BP (Fig. 6). However, contrary to the YLDV tetramer, the human tetramer lost one of its interfaces after removal of the disulfide bond (Fig. 6 – orange). This immediate perturbation to one of the tetramer interfaces may suggest a less stable interface of the human tetramer than that of the YLDV tetramer. In line with this assertion, we observed fewer intermolecular contacts at the human interface than at the YLDV interface (Fig. 5b–c). Nonetheless, the human tetramer stayed intact even after the disruption of one of its interfaces, reflecting the sufficiency of one intact interface for tetramer stability. Thus, we note that the bivalent binding mode of the human tetramer leading to a grid-like organization of heterodimers may provide a stability advantage to the host decoy. In conclusion, our study showed that the IL18-IL18BP complexes, particularly the human complex, can be stabilized by (i) maintaining the helical fold for the surface epitope and reducing backbone fluctuations and (ii) forming a tetrameric assembly. Specifically, these stabilization scenarios are not mutually exclusive; as only when the compact helical fold is lost, the C74 can probe for another thiol group to form a tetrameric assembly.

Data Availability

3D coordinate of the human tetramer structure after equilibration for 60 ns is available from https://github.com/timucinlab/IL18/.

Declaration of Competing Interest

The authors declare that they have no known competing financial interests or personal relationships that could have appeared to influence the work reported in this paper.

Acknowledgments

All of the calculations reported in this paper were performed by the computational resources at TUBITAK ULAKBIM, High Performance and Grid Computing Center (TRUBA resources). This study was partially supported by the European Molecular Biology Organization (EMBO) Installation Grant (IG 4727 to S. Belkaya).

Appendix A. Supporting information

Supplementary data associated with this article can be found in the online version at doi:10.1016/j.csbj.2023.06.021.

References

[1] Abraham MJ, Murtola T, Schulz R, Páll S, Smith JC, Hess B, et al. Gromacs: high performance molecular simulations through multi-level parallelism from laptops to supercomputers. SoftwareX 2015;1:19–25.
[2] Afonina IS, Müller C, Martin SJ, Beyaert R. Proteolytic processing of interleukin-1 family cytokines: variations on a common theme. Immunity 2015;42:991–1004.
[3] Aizawa Y, Akita K, Taniai M, Torigoe K, Mori T, Nishida Y, et al. Cloning and expression of interleukin-18 binding protein. FEBS Lett 1999;445:338–42. https://doi.org/10.1016/s0014-5793(99)00148-9
[4] Baek M, DiMaio F, Anishchenko I, Dauparas J, Ovchinnikov S, Lee GR, et al. Accurate prediction of protein structures and interactions using a three-track neural network. Science 2021;373:871–6.
[5] Bakan A, Bahar I. The intrinsic dynamics of enzymes plays a dominant role in determining the structural changes induced upon inhibitor binding. Proc Natl Acad Sci 2009;106:14349–54.
[6] Bekker H, Berendsen H, Dijkstra E, Achterop S, Vondrumen R, Vanderspoel D, et al., Gromacs–a parallel computer for molecular-dynamics simulations. In: Proceedings of the 4th international conference on computational physics (PC 92). World Scientific Publishing; 1993, p. 252–6.
[7] Belkaya S, Michailidis E, Korol CB, Kabbani M, Cobat A, Bastard P, et al. Inherited IL-18bp deficiency in human fulminant viral hepatitis. J Exp Med 2019;216:1777–90.
[8] Born TL, Morrison LA, Esteban DJ, VandenBos T, Thebeau LG, Chen N, et al. A poxvirus protein that binds to and inactivates IL-18, and inhibits NK cell response. J Immunol 2000;164:3246–54. https://doi.org/10.4049/jimmunol.164.6.3246. [publisher: American Association of Immunologists Section: Host Defense].
[9] Butera D, Cook KM, Chiu J, Wong JW, Hogg PJ. Control of blood proteins by functional disulfide bonds. Blood J Am Soc Hematol 2014;123:2000–7.
[10] Cheong HS, Chang JS, Park JM, Byun SM. Affinity enhancement of bispecific antibody against two different epitopes in the same antigen. Biochem Biophys Res Commun 1990;173:795–800.
[11] Darden T, York D, Pedersen L. Particle mesh ewald: an n log (n) method for Ewald sums in large systems. J Chem Phys 1993;98:10089–92.
[12] Detry S, Andries J, Bloch Y, Gabay C, Clancy DM, Savvides SN. Structural basis of human IL-18 sequestration by the decoy receptor IL-18 binding protein in inflammation and tumor immunity. J Biol Chem 2022:298.
[13] Eastman P, Swails J, Chodera JD, McGibbon RT, Zhao Y, Beauchamp KA, et al. Openmm 7: rapid development of high performance algorithms for molecular dynamics. PLoS Comput Biol 2017;13:e1005659.
[14] Eswar N, Eramian D, Webb B, Shen MY, Sali A. Protein structure modeling with modeller. Structural proteomics. Springer; 2008. p. 145–59.
[15] Evans R, O'Neill M, Pritzel A, Antropova N, Senior A, Green T, et al. Protein complex prediction with alphafold-multimer. BioRxiv 2022. [2021-10].
[16] Gowers RJ, Linke M, Barnoud J, Reddy TJE, Melo MN, Seyler SL, et al., MDAnalysis: a Python package for the rapid analysis of molecular dynamics simulations [Technical Report]. Los Alamos, NM (United States): Los Alamos National Lab. (LANL); 2019.
[17] Grant BJ, Rodrigues APC, ElSawy KM, McCammon JA, Caves LSD. Bio3d: an R package for the comparative analysis of protein structures. Bioinformatics 2006;22:2695–6. https://doi.org/10.1093/bioinformatics/btl461
[18] Hamelberg D, Mongan J, McCammon JA. Accelerated molecular dynamics: a promising and efficient simulation method for biomolecules. J Chem Phys 2004;120:11919–29.
[19] Hansson T, Oostenbrink C, van Gunsteren W. Molecular dynamics simulations. Curr Opin Struct Biol 2002;12:190–6.
[20] Huang J, MacKerell Jr AD. CHARMM36 all-atom additive protein force field: validation based on comparison to NMR data. J Comput Chem 2013;34:2135–45. https://doi.org/10.1002/jcc.23354
[21] Humphrey W, Dalke A, Schulten K. VMD: visual molecular dynamics. J Mol Graph 1996;14(33–38):27–8. https://doi.org/10.1016/0263-7855(96)00018-5
[22] Ihim SA, Abubakar SD, Zian Z, Sasaki T, Saffarioun M, Maleknia S, et al. Interleukin-18 cytokine in immunity, inflammation, and autoimmunity: biological role in induction, regulation, and treatment. Front Immunol 2022:4470.
[23] Jorgensen WL, Chandrasekhar J, Madura JD, Impey RW, Klein ML. Comparison of simple potential functions for simulating liquid water. J Chem Phys 1983;79:926–35. https://doi.org/10.1063/1.445869
[24] Jumper J, Evans R, Pritzel A, Green T, Figurnov M, Ronneberger O, et al. Highly accurate protein structure prediction with alphafold. Nature 2021;596:583–9.
[25] Kaplanski G. Interleukin-18: biological properties and role in disease pathogenesis. Immunol Rev 2018;281:138–53. https://doi.org/10.1111/imr.12616
[26] Kato Z, Jee J, Shikano H, Mishima M, Ohki I, Ohnishi H, et al. The structure and binding mode of interleukin-18. Nat Struct Mol Biol 2003;10:966–71.
[27] Kozakov D, Hall DR, Xia B, Porter KA, Padhorny D, Yueh C, et al. The ClusPro web server for protein-protein docking. Nat Protoc 2017;12:255–78. https://doi.org/10.1038/nprot.2016.169. [number: 2 Publisher: Nature Publishing Group].
[28] Krumm B, Meng X, Li Y, Xiang Y, Deng J. Structural basis for antagonism of human interleukin 18 by poxvirus interleukin 18-binding protein. Proc Natl Acad Sci 2008;105:20711–5. https://doi.org/10.1073/pnas.0809086106. [publisher: Proceedings of the National Academy of Sciences].
[29] Krumm B, Meng X, Wang Z, Xiang Y, Deng J. A unique bivalent binding and inhibition mechanism by the Yatapoxvirus interleukin 18 binding protein. PLoS Pathog 2012;8:e1002876. https://doi.org/10.1371/journal.ppat.1002876. [publisher: Public Library of Science].

[30] Krumm B, Meng X, Xiang Y, Deng J. Identification of small molecule inhibitors of interleukin-18. Sci Rep 2017;7:483. https://doi.org/10.1038/s41598-017-00532-x. [number: 1 Publisher: Nature Publishing Group].
[31] Kuttner YY, Nagar T, Engel S. Surface dynamics in allosteric regulation of protein-protein interactions: modulation of calmodulin functions by Ca^{2+}XXXXXXXXX. PLoS Comput Biol 2013;9:e1003028.
[32] Lindahl E, Hess B, Van Der Spoel D. Gromacs 3.0: a package for molecular simulation and trajectory analysis. Mol Model Annu 2001;7:306–17.
[33] Liu J, Nussinov R. Allostery: an overview of its history, concepts, methods, and applications. PLoS Comput Biol 2016;12:e1004966.
[34] Marti-Renom MA, Yerkovich B, Sali A. Comparative protein structure prediction. Curr Protoc Protein Sci 2002;28:2.9.1–2.9.22. https://doi.org/10.1002/0471140864.ps0209s28
[35] Mühl H, Bachmann M. IL-18/IL-18BP and IL-22/IL-22BP: two interrelated couples with therapeutic potential. Cell Signal 2019;63:109388. https://doi.org/10.1016/j.cellsig.2019.109388
[36] Miao Y, Feher VA, McCammon JA. Gaussian accelerated molecular dynamics: unconstrained enhanced sampling and free energy calculation. J Chem Theory Comput 2015;11:3584–95.
[37] Michaud-Agrawal N, Denning EJ, Woolf TB, Beckstein O. MDAnalysis: a toolkit for the analysis of molecular dynamics simulations. J Comput Chem 2011;32:2319–27. https://doi.org/10.1002/jcc.21787
[38] Miller S, Janin J, Lesk AM, Chothia C. Interior and surface of monomeric proteins. J Mol Biol 1987;196:641–56.
[39] Mirdita M, Schütze K, Moriwaki Y, Heo L, Ovchinnikov S, Steinegger M. Colabfold: making protein folding accessible to all. Nat Methods 2022:1–4.
[40] Mirdita M, Steinegger M, Söding J. Mmseqs2 desktop and local web server app for fast, interactive sequence searches. Bioinformatics 2019;35:2856–8.
[41] Monod J. On the nature of allosteric transitions: a plausible model. J Mol Biol 1965;12:88.
[42] Müller KM, Arndt KM, Plückthun A. Model and simulation of multivalent binding to fixed ligands. Anal Biochem 1998;261:149–58.
[43] Nazarian SH, Rahman MM, Werden SJ, Villeneuve D, Meng X, Brunetti C, et al. Yaba monkey tumor virus encodes a functional inhibitor of interleukin-18. J Virol 2008;82:522–8. https://doi.org/10.1128/JVI.00688-07. [publisher: American Society for Microbiology].
[44] Necci M, Piovesan D, Tosatto SC. Critical assessment of protein intrinsic disorder prediction. Nat Methods 2021;18:472–81.
[45] Novick D, Kim SH, Fantuzzi G, Reznikov LL, Dinarello CA, Rubinstein M. Interleukin-18 binding protein: a novel modulator of the Th1 cytokine response. Immunity 1999;10:127–36. https://doi.org/10.1016/S1074-7613(00)80013-8
[46] Nuara AA, Walter LJ, Logsdon NJ, Yoon SI, Jones BC, Schriewer JM, et al. Structure and mechanism of IFN-γ antagonism by an orthopoxvirus IFN-γ-binding protein. Proc Natl Acad Sci 2008;105:1861–6.
[47] Rose GD, Geselowitz AR, Lesser GJ, Lee RH, Zehfus MH. Hydrophobicity of amino acid residues in globular proteins. Science 1985;229:834–8.
[48] Ruff KM, Pappu RV. Alphafold and implications for intrinsically disordered proteins. J Mol Biol 2021;433:167208.
[49] Shehata M, Ünlü A, Iglesias-Fernández J, Osuna S, Sezerman OU, Timucin E. Brave new surfactant world revisited by thermoalkalophilic lipases: computational insights into the role of SDS as a substrate analog. Phys Chem Chem Phys 2022.
[50] Smith VP, Bryant NA, Alcamí AY. Ectromelia, vaccinia and cowpox viruses encode secreted interleukin-18-binding proteins. J Gen Virol 2023;81:1223–30. https://doi.org/10.1099/0022-1317-81-5-1223. [publisher: Microbiology Society].
[51] Steinegger M, Meier M, Mirdita M, Vöhringer H, Haunsberger SJ, Söding J. Hh-suite3 for fast remote homology detection and deep protein annotation. BMC Bioinform 2019;20:1–15.
[52] Steinegger M, Söding J. Mmseqs2: sensitive protein sequence searching for the analysis of massive data sets. bioRxiv 2017:079681.
[53] Suzek BE, Wang Y, Huang H, McGarvey PB, Wu CH, Consortium U. Uniref clusters: a comprehensive and scalable alternative for improving sequence similarity searches. Bioinformatics 2015;31:926–32.
[54] Tien MZ, Meyer AG, Sydykova DK, Spielman SJ, Wilke CO. Maximum allowed solvent accessibilites of residues in proteins. PLoS One 2013;8:e80635.
[55] Tsutsumi N, Kimura T, Arita K, Ariyoshi M, Ohnishi H, Yamamoto T, et al. The structural basis for receptor recognition of human interleukin-18. Nat Commun 2014;5:5340. https://doi.org/10.1038/ncomms6340. [number: 1 Publisher: Nature Publishing Group].
[56] Van Der Spoel D, Lindahl E, Hess B, Groenhof G, Mark AE, Berendsen HJ. Gromacs: fast, flexible, and free. J Comput Chem 2005;26:1701–18.
[57] Wei H, Wang D, Qian Y, Liu X, Fan S, Yin HS, et al. Structural basis for the specific recognition of IL-18 by its alpha receptor. FEBS Lett 2014;588:3838–43. https://doi.org/10.1016/j.febslet.2014.09.019
[58] Wong JW, Ho SY, Hogg PJ. Disulfide bond acquisition through eukaryotic protein evolution. Mol Biol Evol 2011;28:327–34.
[59] Xiang Y, Moss B. IL-18 binding and inhibition of interferon γ induction by human poxvirus-encoded proteins. Proc Natl Acad Sci 1999;96:11537–42. https://doi.org/10.1073/pnas.96.20.11537. [publisher: Proceedings of the National Academy of Sciences].
[60] Yasuda K, Nakanishi K, Tsutsui H. Interleukin-18 in health and disease. Int J Mol Sci 2019;20:649.
[61] Yasuda K, Nakanishi K, Tsutsui H. Interleukin-18 in health and disease. Int J Mol Sci 2019;20:649. https://doi.org/10.3390/ijms20030649. [number: 3 Publisher: Multidisciplinary Digital Publishing Institute].
[62] Van Zundert GCP, Rodrigues JPGLM, Trellet M, Schmitz C, Kastritis PL, Karaca E, et al. The HADDOCK2.2 web server: user-friendly integrative modeling of biomolecular complexes. J Mol Biol 2016;428:720–5. https://doi.org/10.1016/j.jmb.2015.09.014